Journal of Marine Research, 41, 461–486, 1983

Equatorial ocean response to growing and moving wind systems with application to the Atlantic

by R. H. Weisberg[1] and T. Y. Tang[1]

ABSTRACT

Investigation is made into the response of an equatorial ocean to growing and moving zonal wind systems as motivated by observations of maximum upwelling central to the equatorial Atlantic basin and westward progressing thermal and momentum signatures near the surface. Analytical solutions to the linear, reduced gravity, equatorial β-plane equations of motion subject to a long wave approximation are given for three easterly forcing functions: 1) linearly expanding fetch with constant stress, 2) linearly expanding fetch and stress, and 3) constant fetch and stress, translating westward. The results, as they may relate to the equatorial Atlantic Ocean, are discussed.

1. Introduction

The sea surface temperature, dynamic height, and momentum fields of the equatorial Atlantic Ocean vary seasonally under the influence of the surface trade winds. Many of the observed features of the seasonal variability have been produced by models forced with uniform zonal winds. This paper points out discrepancies that may be associated with the non-uniform manner in which the wind stress intensifies. Investigation is made into the response of an equatorial ocean to zonal wind stress systems which either expand and intensify westward or move westward. Section 2 discusses the motivating observations and previous theoretical work. Attention is drawn toward a region of maximum equatorial upwelling central to the basin, and to westward progressing thermal and momentum signatures observed near the surface. Analytical solutions to the linear equatorial β-plane equations of motion are given in Section 3 for the following easterly forcing functions: 1) linearly expanding fetch with constant stress, 2) linearly expanding fetch and stress, and 3) constant fetch and stress, translating westward. The results, as they may relate to the equatorial Atlantic Ocean, are discussed in Section 4, and the paper is summarized in Section 5.

2. Background

Hastenrath and Lamb (1977) and Hellerman (1979) describe the surface wind field over the equatorial Atlantic Ocean and its seasonal variability using climatically

1. Department of Marine, Earth and Atmospheric Sciences, North Carolina State University, Raleigh, North Carolina, 27650, U.S.A.

averaged ship observations. Northeast and southeast trades, separated by the ITCZ, prevail over the western two thirds of the region while southerlies occupy the Gulf of Guinea. During March, when the ITCZ is at its southernmost position, the equatorial winds are weakest; while during August, when the ITCZ is at its northernmost position, the equatorial winds are strongest.

The ocean responds to the seasonally varying winds by adjusting its near surface pressure field. This occurs nearly in phase with the winds over most of the equatorial Atlantic (Merle, 1978; Katz, 1981; and Katz *et al.*, 1977) while the Pacific, being both larger than and subject to a more complex wind field than the Atlantic, possesses interannual variability in excess of the annual (e.g., Meyers, 1982; Horel, 1982) with extreme conditions giving rise to El Nino occurrences (large-scale warmings in the eastern tropical Pacific).

Analytical and numerical model simulations of the seasonal (or interannual) cycle have generally taken two approaches. The first has been to switch on and off spatially uniform or bounded winds and to observe the thermocline adjustment brought about by free wave propagation. The second, again with spatially uniform or bounded winds, has been to force the equatorial basin periodically and to observe the particular solution at some time beyond the statistical steady state. Examples of the switched on or off experiments include McCreary (1976) and Cane and Sarachik (1976) using reduced gravity equatorial wave models, Hurlburt *et al.* (1976) using a nonlinear reduced gravity numerical model, and Philander and Pacanowski (1980) and Philander (1981) respectively using multilevel nonlinear and linear numerical models. Examples of periodic forcing experiments are Cane and Sarachik (1981) using a reduced gravity equatorial wave model, Busalacchi and O'Brien (1980) using a linear reduced gravity numerical model, and Philander and Pacanowski (1981) using multilevel linear and nonlinear numerical models. Busalacchi and O'Brien (1980, 1981) have also performed linear reduced gravity numerical model integrations using historically derived wind fields. Kelvin and long Rossby waves resulting from the zonal component of the wind stress play the dominant roles in the adjustment process for all of these models.

Several observational comparisons with model results have been undertaken for the Atlantic Ocean. Moore *et al.* (1978) suggested a relationship between temperature fluctuations observed on the equator and at Gulf of Guinea coastal stations by considering the propagation time of an equatorial Kelvin wave. A companion paper by Adamec and O'Brien (1978) provided a numerical integration in support of this theory that Gulf of Guinea upwelling is remotely forced by zonal winds in the western side of the basin. Katz and Garzoli (1982) compared the equatorial velocity profile data set obtained during the Global Weather Experiment with the switched on and off simulations of Philander and Pacanowski (1980) and Philander (1981) respectively and found qualitative similarities in both the build up and relaxation of the surface South Equatorial Current (SEC) and the Equatorial Undercurrent (EUC). Merle's

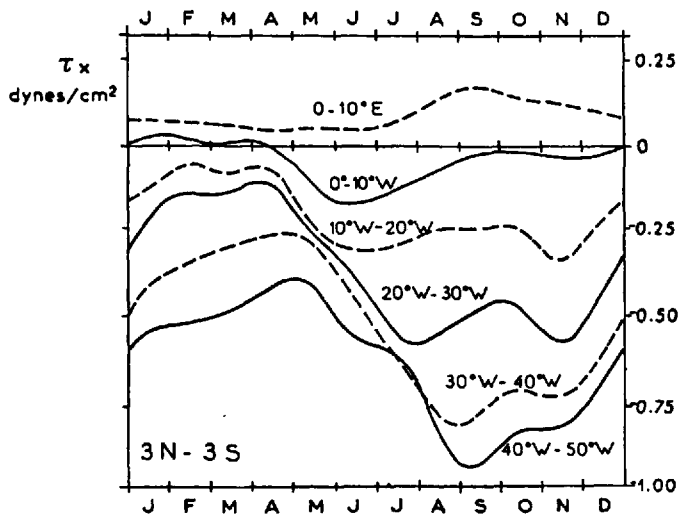

Figure 1. Climatic averaged zonal wind stress component for selected longitude bands between 3N–3S as functions of time using the data set of Hastenrath and Lamb (1977) (from Picaut, 1983).

(1980) analysis of the historical hydrographic data from the NODC files suggested a pivot point about which the equatorial thermocline appeared to oscillate annually, and this compared favorably with Cane and Sarachik's (1981) periodic forcing result.

Observational departures from the model experiments described are expected since the zonal wind stress forcing over the equatorial Atlantic is uniform in neither space nor time. The prime meridian marks a transition along the equator from meridional (southerly) wind stress over the Gulf of Guinea (eastern third of the basin) to a more zonal (southeasterly) wind stress over the western two thirds of the basin. Picaut's (1983) rendition of the Hastenrath and Lamb (1977) data set, given in Figure 1, shows that both the amplitude and phase of the zonal wind stress component's seasonal cycle vary longitudinally. Zonal winds first begin to intensify in the band of 0W–10W around April. This build up progresses both in amplitude and phase to the west whereby a month or so later winds in the band of 30W–40W begin to intensify. Upper ocean thermal and momentum features are now described which may be associated with the wind stress nonuniformities.

The transition region on the equator from meridional to zonal wind stress coincides approximately with a region of both minimum sea surface temperature (SST) in boreal summer and maximum annual SST range. Figure 2 shows the climatic averaged SST field for July with temperature contours highlighted over an equatorial band. The minimum SST during this month occurs between 6W–12W, within which the annual range is around 6°C (Hastenrath and Lamb, 1977). Houghton (1983) shows that this SST variability is associated with a seasonal shoaling of the thermocline, also

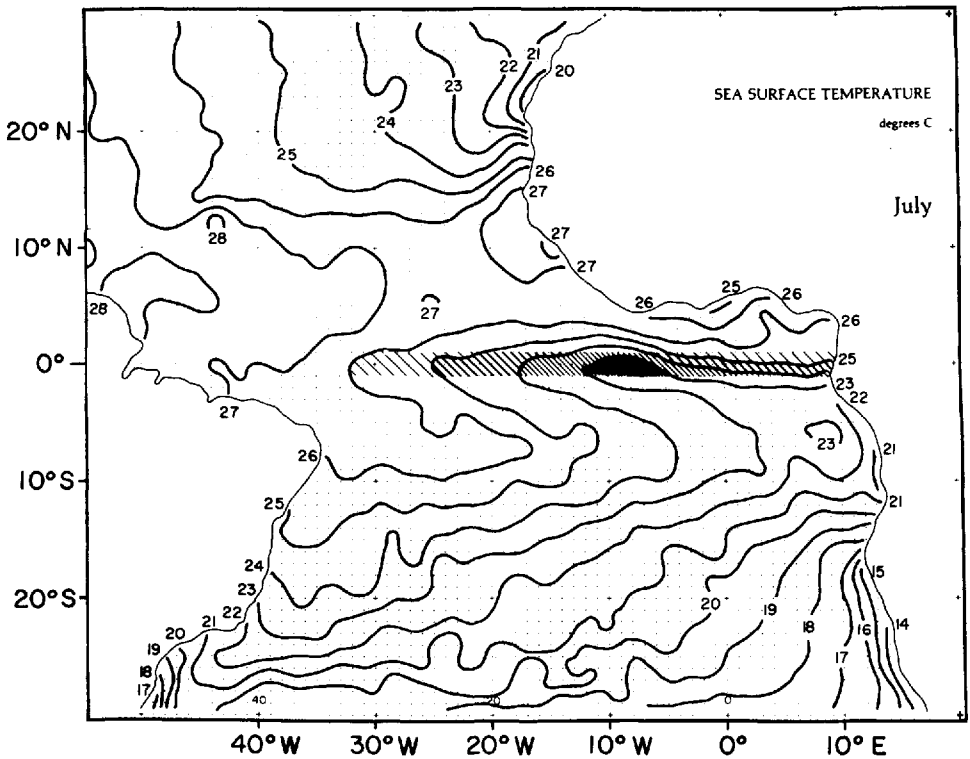

Figure 2. Climatic averaged sea-surface temperature during July highlighted to show the equatorial cold water band (adapted from Hastenrath and Lamb, 1977).

maximum within this region, distinctly separate from the African coast, and both symmetric about and tightly confined to the equator (Fig. 3). We therefore believe this equatorial cold water to be primarily of upwelling and vertical mixing origin. It is further suggested, by an Inverted Echo Sounder (IES) record from 0N, 4W given in Figure 4, that the seasonal upwelling occurs quite rapidly. An abrupt rise in the thermocline spanning a period of about one month from March to April is inferred from the increase in acoustic travel time.

Paralleling the westward progression of the zonal wind stress, recent surface moored current meter measurements from the central equatorial Atlantic show evidence of westward-progressing thermal and momentum events in the surface layer. Figure 5 shows low-pass filtered eastward velocity component and temperature time series obtained using Vector Averaging Current Meters at depths of 10 m and 100 m on taut wire surface moorings on the equator at 24W and 26W. At the 10 m level around May, the SST begins to drop and the SEC accelerates westward, both being consistent with an increasing westward zonal wind stress component. The SEC intensifies through mid-June at which time SST increases abruptly followed immediately by an equally

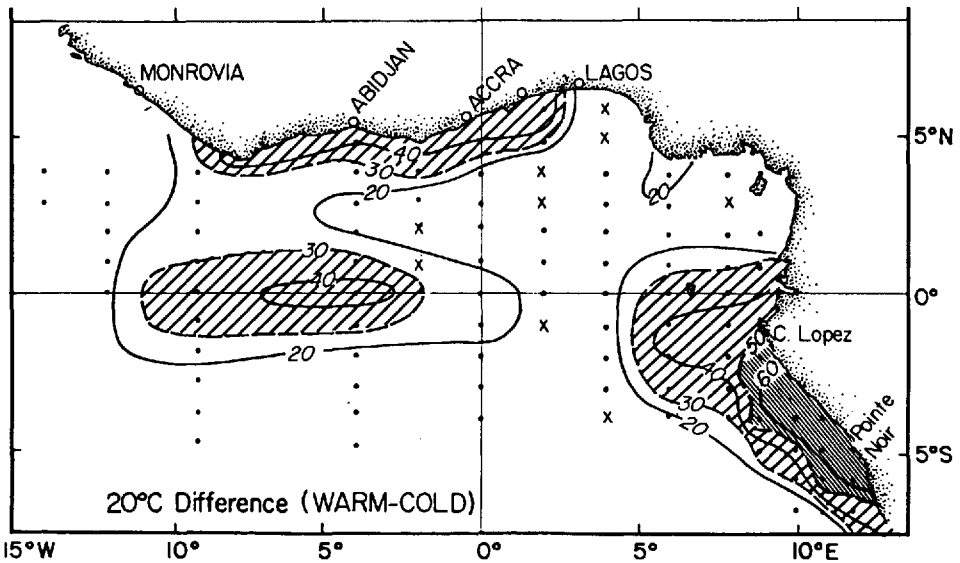

Figure 3. Vertical displacement in meters for the 20°C isotherm between the warm and cold seasons (boreal spring and summer respectively) computed from historical data. Cross-hatched areas denote regions of upwelling (from Houghton, 1983).

abrupt decrease. Simultaneous with the abrupt SST increase is a further westward acceleration of the SEC, followed immediately by a reversal of momentum from westward to eastward; i.e., the EUC appears to have surfaced. Correlating the records at both stations shows that the momentum and thermal events at 24W lead those at 26W by around 2.3 days. This gives a westward progression of 110 cm/sec which does not correspond to a free baroclinic wave phase speed. The velocity sensors failed shortly after the event; however, it would appear that the SEC has been greatly diminished at the equator even though the southeasterly trades (as speculated on by the climatic mean) should be at their maximum intensity.

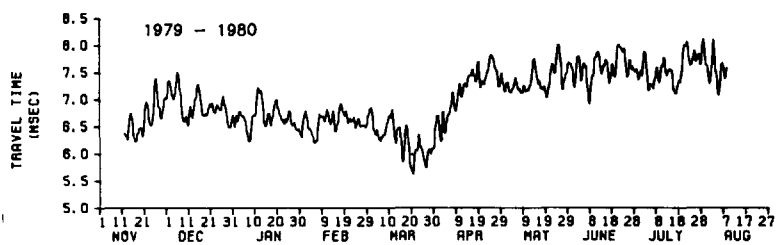

Figure 4. Acoustic travel time measured by an Inverted Echo Sounder at 0N, 4W from Nov. 1979–Aug. 1980. The slope of a linear regression between the depth of the 20°C isotherm and the travel time determined using repeated STD casts was −18m/msec (courtesy of L. Miller).

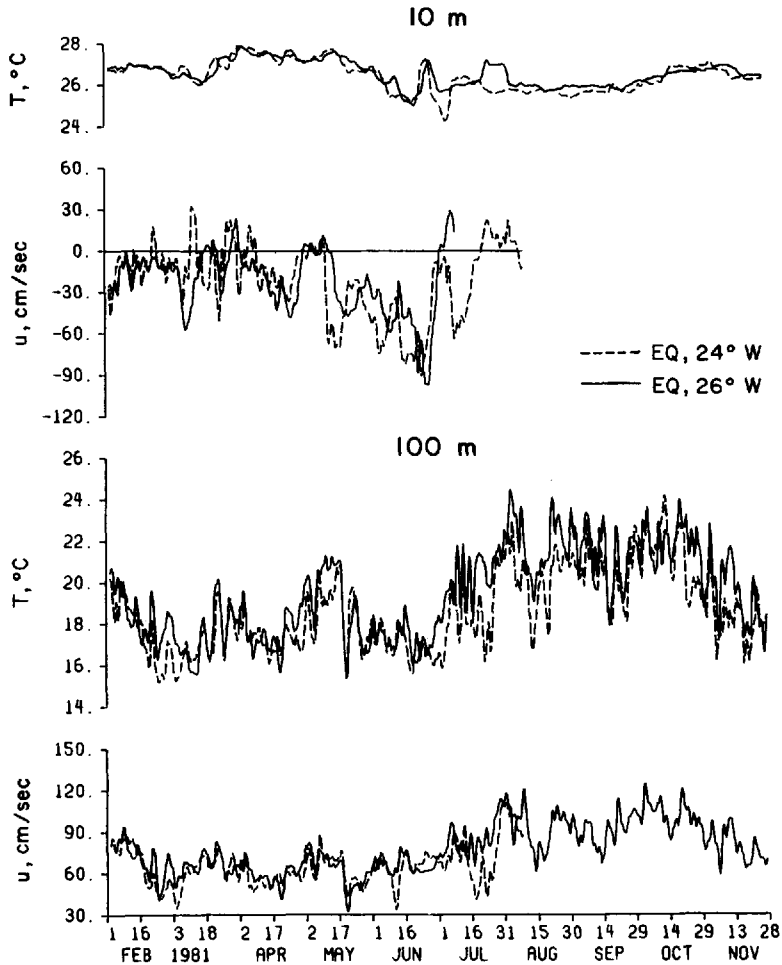

Figure 5. Low-pass filtered temperature and velocity components observed at depths of 10 m and 100 m along the equator at 26W (solid line) and 24W (dashed line).

The records near the core of the EUC at 100 m though aliased by higher frequency oscillations show a more gradual increase in temperature and eastward momentum beginning in July with increased values lasting on through October when the winds presumably began to abate. The progression at this level is from west to east (opposite that of the surface) at a rate of around 160 cm/sec. Calculating a reduced gravity Kelvin wave speed based upon the density difference across the base of the mixed layer (3 sigma-*t* units) which we've been referring to as the thermocline and its mean depth (90 m) as observed during the mooring deployment and recovery cruises, we also arrive at 160 cm/sec in agreement with the above. The thermal and momentum features at 100 m lag those at 10 m by more than a week at both longitudes; it will be suggested in

Section 4 that this results from independent processes occurring at both levels as opposed to local vertical propagation.

Attention has now been drawn upon two features. 1) The minimum SST and maximum SST annual variation along the equator in the Atlantic both occur between 6W–12W. This appears to be of equatorial upwelling origin with the thermocline raising some 40 m over a one month period during boreal spring. 2) Westward progressing thermal and momentum features are observed near the surface in the western portion of the equatorial Atlantic at the time when the climatic averaged zonal wind stress component reaches its maximum value. These features occurred very abruptly and travelled at a speed which did not coincide with a free baroclinic equatorial wave speed.

3. Analytical results

The premise to be investigated is that some portion of the thermocline adjustment may be induced internal to the basin as opposed to propagated in from meridional boundaries. Particular emphasis is given to the role of equatorial Rossby wave fronts as motivated by observations of westward progressing thermal and momentum events. Three different easterly wind stress forcing functions are considered over an unbounded basin: 1) winds of constant amplitude with fetch growing linearly to the west, 2) winds with both amplitude and fetch growing linearly to the west, and 3) winds of both constant amplitude and fetch translating westward.

Consider a two layer reduced gravity model on an equatorial β-plane, nondimensionalized by a horizontal length scale $L = (g'H_o)^{1/4}/\beta^{1/2}$ and a time scale $T = (g'H_o)^{-1/4} \cdot \beta^{-1/2}$, where g' is the reduced gravity and H_o is the mean thermocline depth. The equations of motion describing perturbations about a basic state of rest are:

$$\frac{\partial u}{\partial t} - yv + \frac{\partial h}{\partial x} = \tau \tag{1}$$

$$\frac{\partial v}{\partial t} + yu + \frac{\partial h}{\partial y} = 0 \tag{2}$$

$$\frac{\partial h}{\partial t} + \frac{\partial u}{\partial x} + \frac{\partial v}{\partial y} = 0 \tag{3}$$

where x, y, and t are the zonal, meridional, and temporal coordinates; u, v, and h are the zonal and meridional velocity components and upper layer thickness respectively; and τ is the zonal forcing function. Cane and Sarachik (1976) discuss the solution to the linear forced equatorial wave problem. Their techniques are directly applicable here. The forcing function is first Fourier transformed in x and then projected onto the free equatorial wave modes which form a complete orthogonal set over the interval between $y = \pm\infty$. The coefficients of the forced equatorial wave response are calculated

from the forcing function coefficients by integrating over time beginning with the initial conditions $u = v = h = 0$ at $t = 0$. The resulting Fourier transforms are then inverted to obtain the solutions in real space. A long wave approximation for Rossby waves is made in this latter step yielding a solution consisting entirely of nondispersive waves.

Since the solutions are in terms of the free equatorial wave modes a brief review of them is in order. The homogeneous equations (1)–(3), with dependent variables proportional to $\exp\{i(kx - \omega t)\}$, where k and ω are the zonal wavenumber component and frequency respectively, may be reduced to a single equation in v:

$$\frac{d^2v}{dy^2} + (\omega^2 - k^2 - k/\omega - y^2)v = 0. \tag{4}$$

The dispersion relation

$$\omega^2 - k^2 - k/\omega = 2n + 1 \tag{5}$$

results from the boundary conditions that v approaches zero as y approaches $\pm\infty$, and the corresponding eigenfunctions are:

$$v_n(y) = \psi_n(y) = (2^n n! \sqrt{\pi})^{-1/2} e^{-y^2/2} H_n(y), \tag{6}$$

where $n \geq 1$ is an integer meridional mode number and $H_n(y)$ are the Hermite Polynomials (e.g. Matsuno, 1966). Two additional special solutions exist: the Kelvin wave ($n = -1$) for which $\omega = k$ and v is identically zero, and the Rossby-gravity wave ($n = 0$) for which $\omega - 1/\omega = k$. For $n \geq 1$, the waves are either Rossby waves or inertia-gravity waves. The former are quasi-geostrophic low-frequency waves whose dispersion relation simplifies in the long wave limit to $\omega = -k/(2n + 1)$. The latter are ageostrophic high-frequency waves.

Forcing functions symmetric about the equator will project only onto even Hermite polynomials. The u and h fields have opposite symmetry from the v field so only odd numbered waves are excited by symmetric zonal forcing. Convergence of the eigenfunction expansion and consequently the number of modes required depends upon the meridional scale of the forcing. Since the response at the equator is primarily due to the lowest modes and since tapering the forcing function to zero away from the equator does not appreciably affect the lowest modes (Cane and Sarachik, 1976) we retain only the Kelvin wave and first Rossby wave in our solutions. This simplification will be justified further under "Case a" below.

Three different symmetric easterly forcing functions are now considered. Kelvin and Rossby wave responses are shown separately and then added together. Since we are most interested in the response at the equator, the meridional velocity component, which is identically zero at the equator for odd Rossby waves, and zero everywhere for Kelvin waves, is omitted. Prior to the introduction of equatorially trapped wave theory,

Ichiye (1959) had considered the response of an equatorial β-plane ocean to a travelling disturbance by neglecting the Coriolis parameter and forcing with a divergent meridional wind stress component at specified frequency and wavenumber. While his focus was upon gravity waves, Ichiye pointed out resonant excitation of Rossby waves for westward moving disturbances. Such resonant behavior will appear in the three cases treated below.

Case a: Constant amplitude stress with fetch growing linearly to the west

The forcing function takes the form:

$$\tau(x, y, t) = -\gamma \exp(-b^2 y^2)\, H(x + \alpha t)\, H(-x), \tag{7}$$

where the H's are step functions, equaling zero or one for negative and positive arguments respectively, α is the fetch expansion rate taken as positive in this formulation, b determines the meridional scale, and γ sets the magnitude of the zonal wind stress. The Kelvin wave ($n = -1$) solution is:

$$u_{-1}(x, y, t) = h_{-1}(x, y, t) = \frac{\gamma \sqrt{2}\, \pi^{1/4}}{2(1 + 2b^2)^{1/2}} \psi_o(y) \cdot \left\{ xH(x) - \frac{(x + \alpha t)H(x + \alpha t)}{1 + \alpha} - \frac{\alpha(x - t)\, H(x - t)}{1 + \alpha} \right\}. \tag{8}$$

Defining

$$A_n = \begin{cases} \dfrac{\gamma \pi^{1/4} (1 - 2b^2)^{(n-1)/2}}{2(n!)^{1/2}(1 + 2b^2)^{n/2}} \left[\dfrac{n(1 - 2b^2)}{(n + 1)(1 + 2b^2)} - 1 \right], & \text{even } n \\ 0, & \text{odd } n \end{cases} \tag{9}$$

the Rossby wave solutions are:

$$\begin{bmatrix} u_n(x, y, t) \\ h_n(x, y, t) \end{bmatrix} = A_n \left\{ \frac{(2n + 1)\alpha(x + t/(2n + 1))H(x + t/(2n + 1))}{\alpha - 1/(2n + 1)} - 2(n + 1)xH(x) - \frac{(x + \alpha t)H(x + \alpha t)}{\alpha - 1/(2n + 1)} \right\} \cdot \begin{bmatrix} -\dfrac{2n + 2}{2n + 1} \sqrt{\dfrac{n}{2}}\, \psi_{n-1}(y) + \dfrac{2n}{2n + 1} \sqrt{\dfrac{n + 1}{2}}\, \psi_{n+1}(y) \\ \dfrac{2n + 2}{2n + 1} \sqrt{\dfrac{n}{2}}\, \psi_{n-1}(y) + \dfrac{2n}{2n + 1} \sqrt{\dfrac{n + 1}{2}}\, \psi_{n+1}(y) \end{bmatrix}, \tag{10}$$

and in the limit that $\alpha = 1/(2n+1)$, using l' Hôspital's rule, these become:

$$\begin{bmatrix} u_n(x,y,t) \\ h_n(x,y,t) \end{bmatrix} = A_n\{(2n+1)xH(x+t/(2n+1)) - (2n+1)xH(x)\}$$
$$\alpha = 1/(2n+1)$$
$$\cdot \begin{bmatrix} -\frac{2n+2}{2n+1}\sqrt{\frac{n}{2}}\psi_{n-1}(y) + \frac{2n}{2n+1}\sqrt{\frac{n+1}{2}}\psi_{n+1}(y) \\ \frac{2n+2}{2n+1}\sqrt{\frac{n}{2}}\psi_{n-1}(y) + \frac{2n}{2n+1}\sqrt{\frac{n+1}{2}}\psi_{n+1}(y) \end{bmatrix}. \quad (11)$$

For the case $n = 1$, Eqs. (10) and (11) may be rewritten as:

$$\begin{bmatrix} u_1(x,y,t) \\ h_1(x,y,t) \end{bmatrix} = A_1\left\{\frac{3\alpha(x+t/3)\,H(x+t/3)}{\alpha - 1/3} - 3xH(x) - \frac{(x+\alpha t)\,H(x+\alpha t)}{\alpha - 1/3}\right\}$$
$$\cdot \begin{bmatrix} \frac{-2\sqrt{2}}{3}\psi_o(y) + \frac{2}{3}\psi_2(y) \\ \frac{2\sqrt{2}}{3}\psi_o(y) + \frac{2}{3}\psi_2(y) \end{bmatrix} \quad (12)$$

and

$$\begin{bmatrix} u_1(x,y,t) \\ h_1(x,y,t) \end{bmatrix} = A_1\{3xH(x+t/3) - 3xH(x)\} \begin{bmatrix} \frac{-2\sqrt{2}}{3}\psi_o(y) + \frac{2}{3}\psi_2(y) \\ \frac{2\sqrt{2}}{3}\psi_o(y) + \frac{2}{3}\psi_2(y) \end{bmatrix} \quad (13)$$
$$\alpha = 1/3$$

respectively. Figures 6–8 show the Kelvin, the $n = 1$ Rossby, and Kelvin plus the $n = 1$ Rossby wave solutions evaluated at the equator with $b = 0$ (meridionally uniform wind stress). Three different fetch expansion rates are used: $\alpha = 1/6, 1/3, 1/2$; corresponding to expansion slower than, equal to, and faster than the Rossby wave group speed. Distributions of u and h are shown as a function of x at nondimensional time $t = 15$ and as a function of t at nondimensional position $x = -5$. With $(g'H_o)^{1/2} = 160$ cm/sec, the time and length scales are $T = 1.91$ days and $L = 264$ km respectively. Thus, $t = 15$ and $x = -5$ correspond to 29 days and 1300 km respectively.

The Kelvin wave u and h fields are identical, and since the energy flux is eastward, varying the westward expansion rate does not affect the character of the solution. Waves are generated within the forced region. Consequently, the response increases from zero at the leading edge to a maximum at the origin and decreases to zero at the

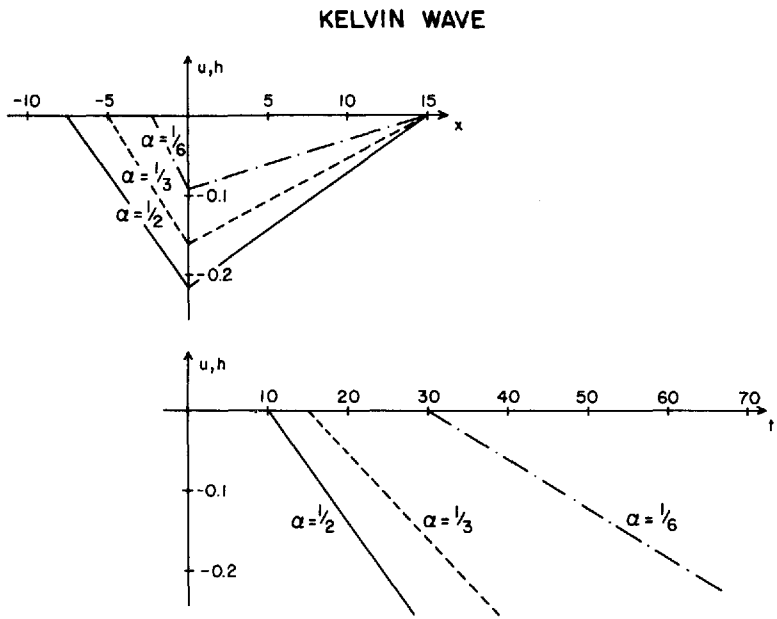

Figure 6. Kelvin wave response in zonal velocity component, u, and upper layer thickness, h, evaluated on the equator for an easterly wind stress with fetch expanding westward at rate α. Curves are given for u and h as functions of x at time $t = 15$, and as functions of time at position $x = -5$ for three different expansion rates: $\alpha = 1/6, 1/3$, and $1/2$.

point $x = t$, since the nondimensional Kelvin wave group speed is unity. Secular growth occurs throughout the field as the forcing region expands.

The Rossby wave response differs since its group speed is westward and equal to $1/3$. The response is always zero at the origin. When $\alpha < 1/3$ the response is maximum at the leading edge of the forced region, decreasing to zero at the point $x = -t/3$. When $\alpha = 1/3$ the waves cannot outrun the forcing so energy collects at the leading edge and abruptly goes to zero beyond. When $\alpha > 1/3$ the waves cannot keep up with the forcing so the maximum response occurs at $x = -t/3$. Note that the u and h responses have opposite signs which differ from the Kelvin wave. The growth curves are also different. No response is evident until the leading edge of the forcing reaches a given point. Secular growth then occurs over the time it takes for the leading edge of the Rossby wave packet to pass by that point. When $\alpha = 1/3$ the growth is instantaneous. After the leading edge of the Rossby wave packet passes a given point, the response remains fixed, since the fetch relative to that point is fixed.

Summing the Kelvin and Rossby wave responses as shown in Figure 8 gives the total long wave response (neglecting higher modes). East of the origin $x = 0$, the response is purely Kelvin, while west of the origin, the response is both Kelvin and Rossby. Of particular interest are the signatures at both ends of the forced region. As the

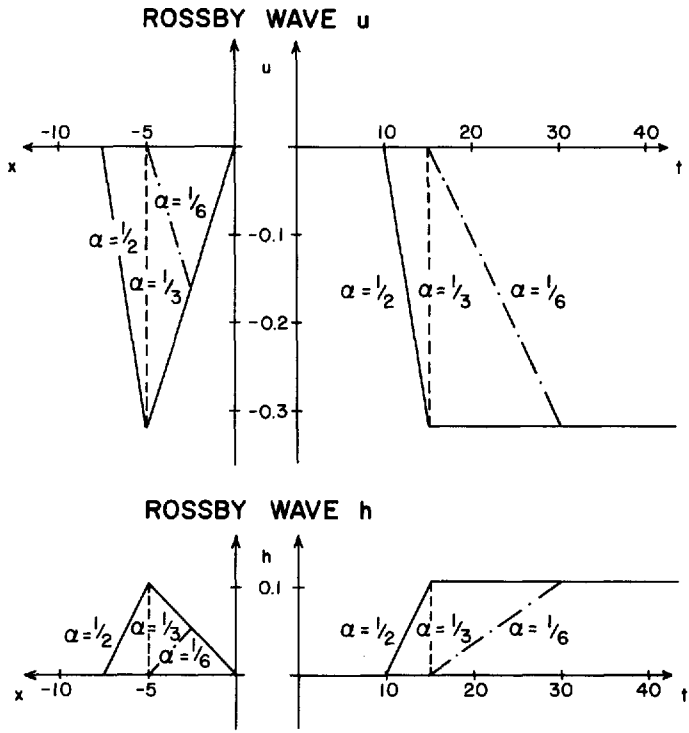

Figure 7. Rossby wave ($n = 1$) response in zonal velocity component, u, and upper layer thickness, h, evaluated on the equator for an easterly wind stress with fetch expanding westward at rate α. Curves are given for u and h as functions of x at time $t = 15$, and as functions of time at position $x = -5$ for three different expansion rates: $\alpha = 1/6, 1/3$, and $1/2$.

expanding edge passes a point, the upper layer first thickens (the thermocline goes down) followed by a thinning (the thermocline goes up). The abruptness over which this occurs depends upon how close the fetch growth rate α is to the Rossby wave group speed. An internal bore is approached as the group speed and expansion rates become equal. At the origin, the thermocline shoals linearly as long as the fetch keeps expanding.

A qualitative explanation of the two features pointed out in Section 2 is thus afforded. 1) Maximum equatorial upwelling of the thermocline between 6W–12W, beginning in boreal spring, corresponds in position and time with the origin of the zonal wind stress component and the onset of its seasonal increase respectively. 2) As the fetch expands we would expect to see abrupt downwelling (SST increase) and westward momentum increase followed by an equally abrupt upwelling (SST decrease) and westward momentum decrease characteristic of the forced Rossby wave front.

Inclusion of higher mode Rossby waves does not qualitatively alter the results as

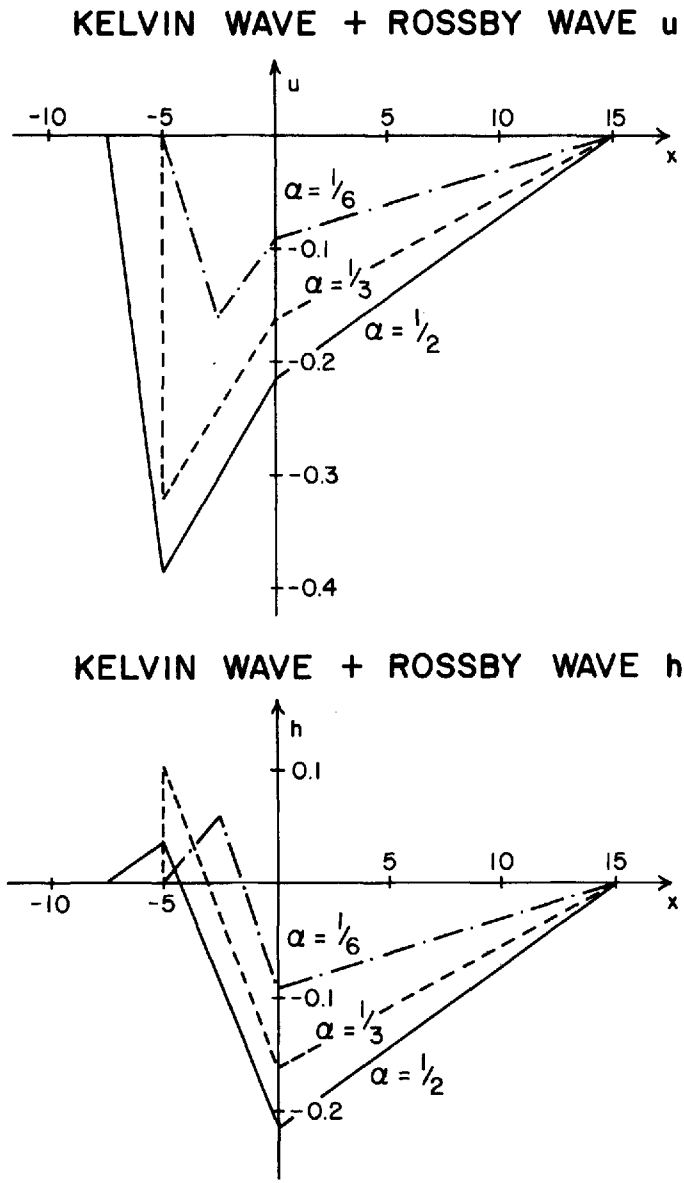

Figure 8. Sum of the Kelvin and Rossby ($n = 1$) wave responses in zonal velocity component, u, and upper layer thickness, h, evaluated on the equator for an easterly wind stress with fetch expanding westward at a rate α. Curves are given for u and h as functions of x at time $t = 15$ for three different expansion rates: $\alpha = 1/6, 1/3$, and $1/2$.

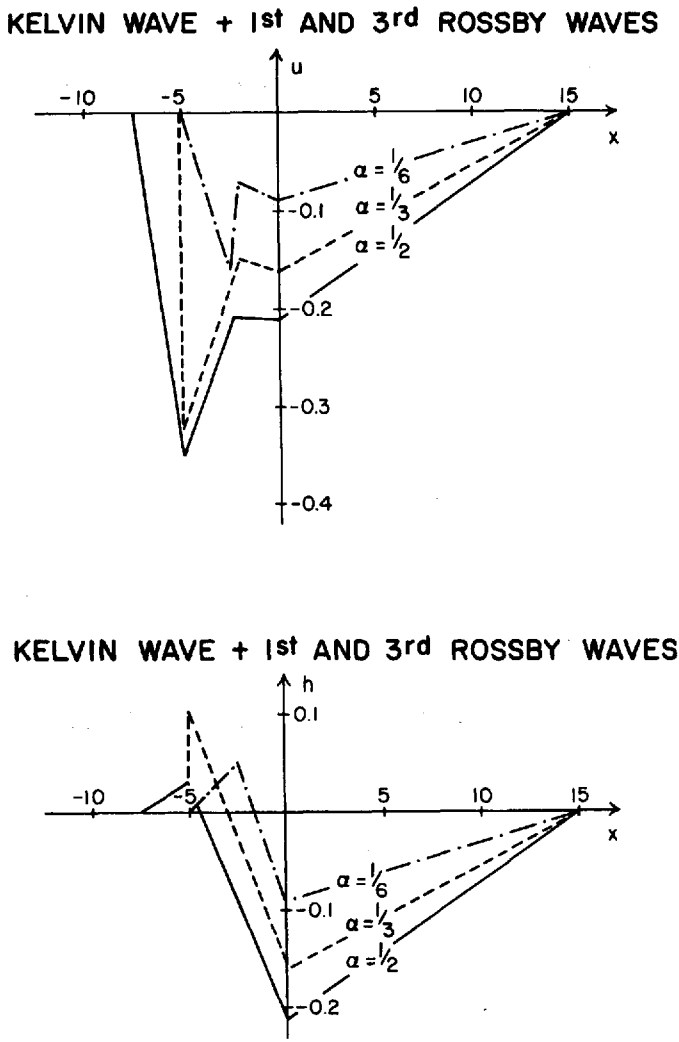

Figure 9. Sum of the Kelvin plus the $n = 1$ and $n = 3$ Rossby wave responses in zonal velocity component, u, and upper layer thickness, h, evaluated on the equator for an easterly wind stress with fetch expanding westward at a rate α. Curves are given for u and h as functions of x at time $t = 15$ for three different expansion rates: $\alpha = 1/6$, $1/3$, and $1/2$.

shown in Figure 9 which is similar to Figure 8 with the addition of the $n = 3$ Rossby wave. Since the $n = 3$ as well as all higher mode Rossby waves travel at slower group speeds, their effects occur only between the leading edge of the dominant $n = 1$ wave and the origin. In this particular case the $n = 3$ wave has opposite sign from the $n = 1$. The u response is lessened by a small amount while the changes in h are nearly imperceptible.

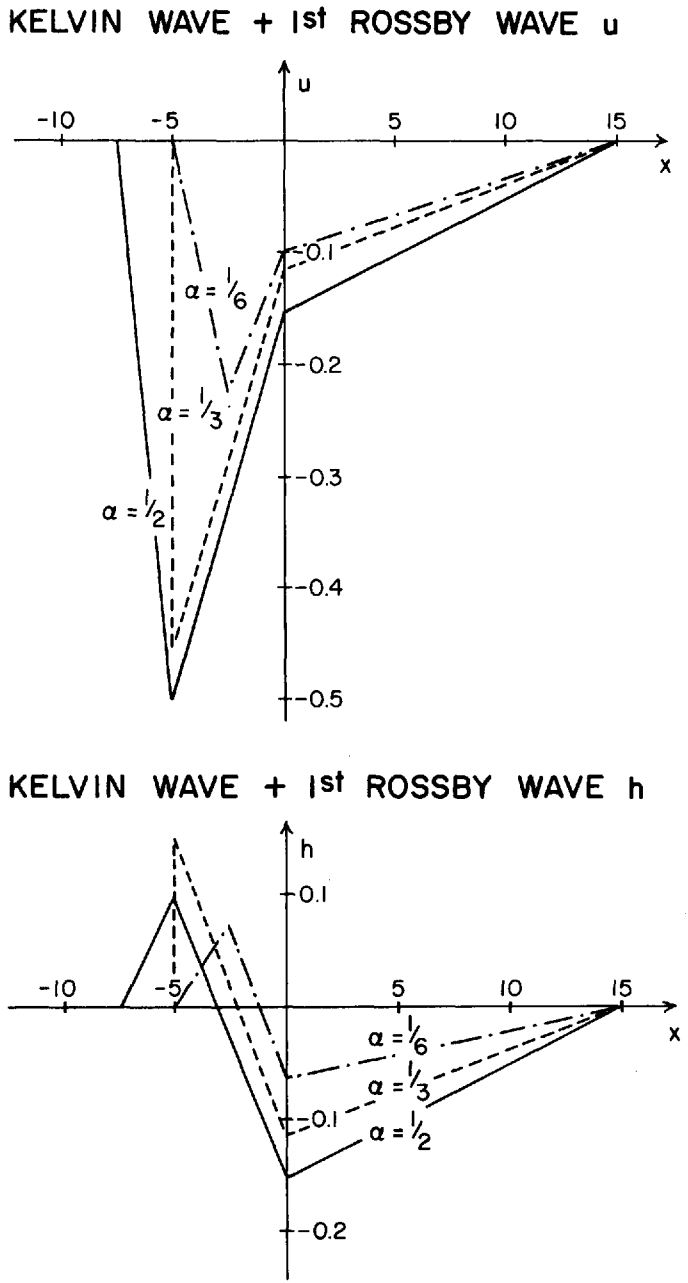

Figure 10. Sum of the Kelvin plus the $n = 1$ and $n = 3$ Rossby wave responses in zonal velocity component, u, and upper layer thickness, h, evaluated on the equator for an easterly wind stress proportional to $e^{y^2/2}$ with fetch expanding westward at a rate α. Curves are given for u and h as functions of x at time $t = 15$ for three different expansion rates: $\alpha = 1/6$, $1/3$, and $1/2$.

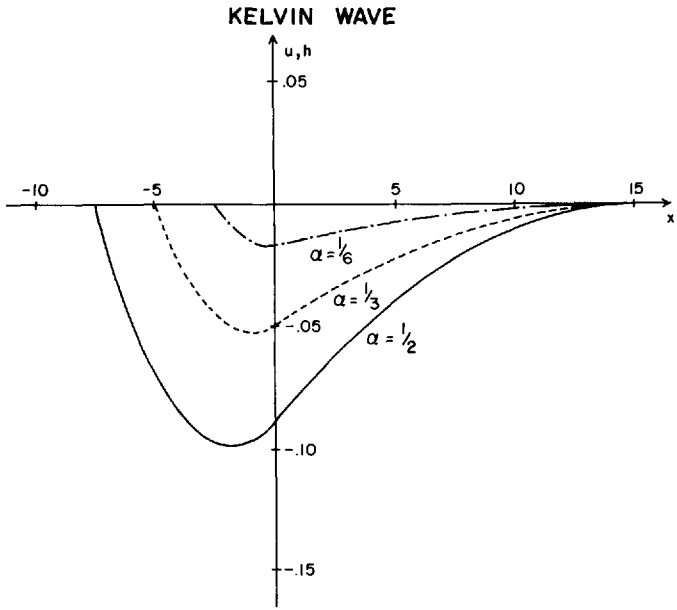

Figure 11. Kelvin wave response in zonal velocity component, u, and upper layer thickness, h, evaluated on the equator for an easterly wind stress with fetch and amplitude growing linearly to the west. Curves are given for u and h as functions of x at $t = 15$ for $\alpha = 1/6$, $1/3$, and $1/2$.

Tapering the forcing function to zero meridionally is also of little qualitative consequence as shown in Figure 10 which is similar to Figure 8 with $b^2 = 0.5$. This is a special case for which the zonal wind stress has the same meridional dependence as $\psi_o(y)$. Therefore it projects only onto the Kelvin and $n = 1$ Rossby waves. All higher mode Rossby waves are identically zero. Since the coefficients are changed so are the amplitudes of their sums but again the qualitative similarity between Figures 10 and 8 is obvious. The choice of $b^2 = 0.5$ is physically reasonable since, with $L = 264$ km, it corresponds to an $e^{-\pi}$ scale of 6° which is approximately the annual mean position of the ITCZ in the central Atlantic. This is not crucial however since other reasonable choices of the parameter b^2 between 0 and $1/2$ give results intermediate between Figures 9 and 10.

Omission of the short Rossby waves, according to Cane and Sarachik (1976), amounts to neglecting a Gibbs effect which again does not qualitatively alter the long wave results. We refer to their Figure 6.

Case b: Fetch and amplitude growing linearly to the west

Figure 1 shows that the amplitude of the zonal wind stress increases as the fetch expands. This may be modelled as:

$$\tau(x, y, t) = -\gamma \exp(-b^2 y^2)\, x\, H(x + \alpha t)\, H(-x). \tag{14}$$

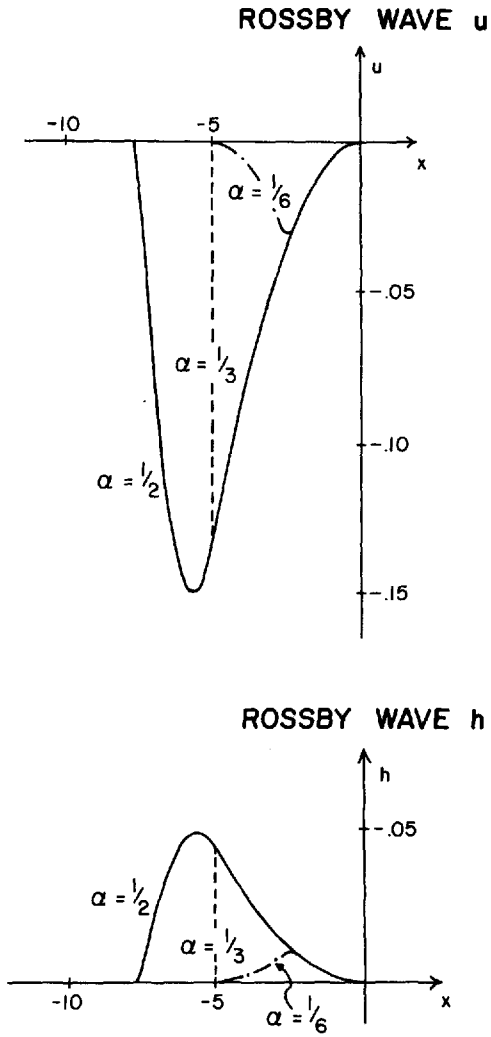

Figure 12. Rossby wave ($n = 1$) response in zonal velocity component, u, and upper layer thickness, h, evaluated on the equator for an easterly wind stress with fetch and amplitude growing linearly to the west. Curves are given for u and h as functions of x at $t = 15$ for $\alpha = 1/6$, $1/3$, and $1/2$.

The solutions are:

$$u_{-1}(x, y, t) = h_{-1}(x, y, t) = \frac{\gamma\sqrt{2}\pi^{1/4}}{2(1 + 2b^2)^{1/2}}\psi_o(y)$$

$$\left\{-\frac{x^2H(x)}{2} + \frac{\alpha^2(x - t)^2\,H(x - t)}{2(\alpha + 1)^2} - \frac{(x + \alpha t)[\alpha t - x(2\alpha + 1)]\,H(x + \alpha t)}{2(\alpha + 1)^2}\right\} \quad (15)$$

for the Kelvin wave, and

$$\begin{bmatrix} u_1(x,y,t) \\ h_1(x,y,t) \end{bmatrix} = A_1 \left\{ \frac{3x^2 H(x)}{2} - \frac{3\alpha^2 (x + t/3)^2 H(x + t/3)}{2(\alpha - 1/3)^2} \right.$$
$$\left. - \frac{(x + \alpha t)(x/3 - 2x\alpha - \alpha t/3) H(x + \alpha t)}{2(\alpha - 1/3)^2} \right\} \cdot \begin{bmatrix} \frac{-2\sqrt{2}}{3}\psi_o(y) + \frac{2}{3}\psi_2(y) \\ \frac{2\sqrt{2}}{3}\psi_o(y) + \frac{2}{3}\psi_2(y) \end{bmatrix} \quad (16)$$

for the first mode Rossby wave, which reduces, in the limit $\alpha = 1/3$, to:

$$\begin{bmatrix} u_1(x,y,t) \\ h_1(x,y,t) \end{bmatrix}_{\alpha = 1/3} = \frac{A_1}{2} \{3x^2 H(x) + 3x^2 H(x + t/3)\} \cdot \begin{bmatrix} \frac{-2\sqrt{2}}{3}\psi_o(y) + \frac{2}{3}\psi_2(y) \\ \frac{2\sqrt{2}}{3}\psi_o(y) + \frac{2}{3}\psi_2(y) \end{bmatrix}. \quad (17)$$

Kelvin, $n = 1$ Rossby, and Kelvin plus $n = 1$ Rossby wave solutions evaluated at $y = 0$ with $b = 0$ are shown in Figures 11–13 for the three different expansion rates. The solutions are qualitatively similar to the simpler case of constant amplitude. One significant difference is that both the Kelvin and Rossby wave maxima are shifted westward since the centroid of the wind stress distribution is now westward of the fetch center. This feature agrees with the observation that the region of SST minimum at 6W–12W is westward of the zonal wind stress component origin which, according to Hastenrath and Lamb (1977) or Figure 1, is closer to the prime meridian.

Case c: Westward translating zonal wind system with constant fetch and amplitude

For this case we choose a forcing function of the form:

$$\tau(x,y,t) = -\gamma \exp(-b^2 y^2) \{H(x + \alpha t + L) - H(x + \alpha t)\}, \quad (18)$$

where L is the zonal extent of a forced region translating westward at speed α. Gill and Schumann (1974) studied an analogous situation in the forcing of continental shelf waves. The equatorial Kelvin and $n = 1$ Rossby wave solutions are:

$$u_{-1}(x,y,t) = h_{-1}(x,y,t) = \frac{\gamma\sqrt{2}\pi^{1/4}}{2(\alpha + 1)(1 + 2b^2)^{1/2}} \psi_o(y)$$
$$\{(x + \alpha t) H(x + \alpha t) - (x - t) H(x - t) - (x + \alpha t + L)$$
$$H(x + \alpha t + L) + (x - t + L) H(x - t + L)\}, \quad (19)$$

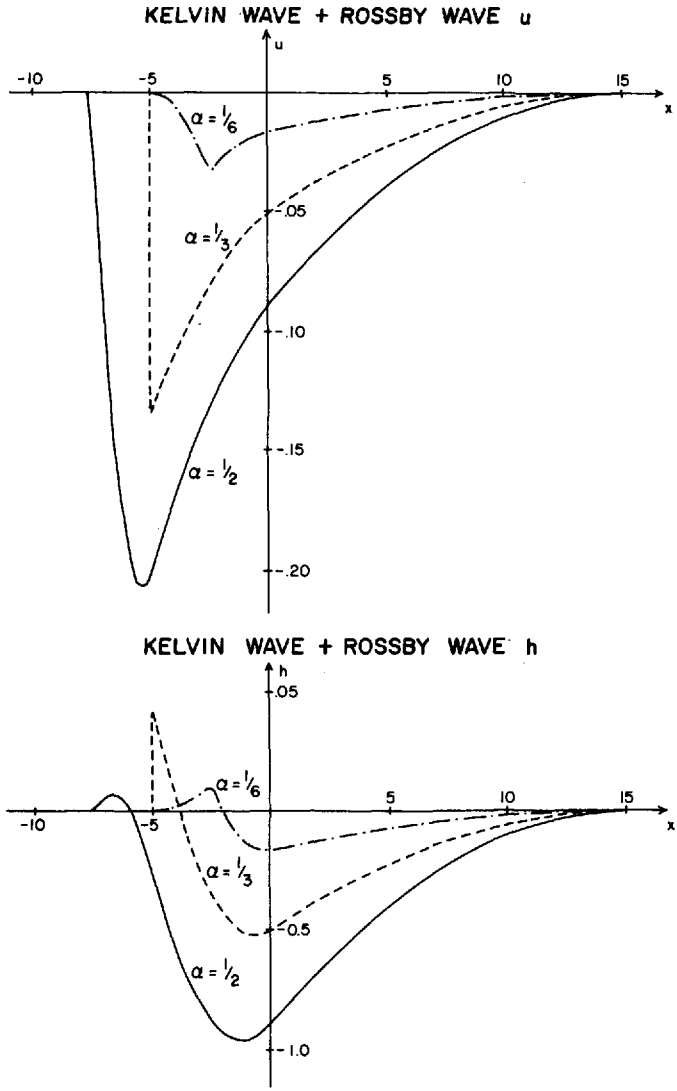

Figure 13. Sum of the Kelvin and Rossby ($n = 1$) wave responses in zonal velocity component, u, and upper layer thickness, h, evaluated on the equator for an easterly wind stress with fetch and amplitude growing linearly to the west. Curves are given for u and h as functions of x at $t = 15$ for $\alpha = 1/6$, $1/3$, and $1/2$.

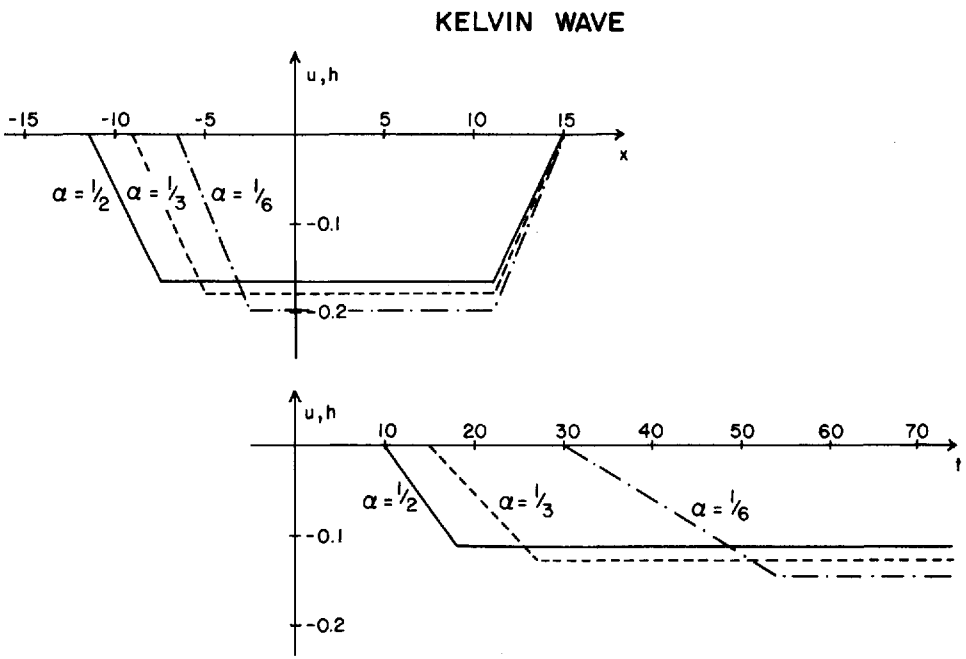

Figure 14. Kelvin wave response in zonal velocity component, u, and upper layer thickness, h, evaluated on the equator for an easterly wind stress with constant amplitude and fetch moving westward at a rate α. Curves are given for u and h as functions of x at $t = 15$ for $\alpha = 1/6$, $1/3$ and $1/2$.

and

$$\begin{bmatrix} u_1(x,y,t) \\ h_1(x,y,t) \end{bmatrix} = \frac{A_1}{(\alpha - 1/3)} \{(x + t)H(x + \alpha t) - (x + t/3)H(x + t/3) - (x + \alpha t + L)H(x + \alpha t + L) + (x + t/3 + L)H(x + t/3 + L)\} \cdot \begin{bmatrix} \frac{-2\sqrt{2}}{3}\psi_o(y) + \frac{2}{3}\psi_2(y) \\ \frac{2\sqrt{2}}{3}\psi_o(y) + \frac{2}{3}\psi_2(y) \end{bmatrix}, \tag{20}$$

which reduces, in the limit $\alpha = 1/3$, to:

$$\begin{bmatrix} u_1(x,y,t) \\ h_1(x,y,t) \end{bmatrix}_{\alpha = 1/3} = A_1 t \{H(x + t/3) - H(x + t/3 + L)\} \begin{bmatrix} \frac{-2\sqrt{2}}{3}\psi_o(y) + \frac{2}{3}\psi_2(y) \\ \frac{2\sqrt{2}}{3}\psi_o(y) + \frac{2}{3}\psi_2(y) \end{bmatrix}. \tag{21}$$

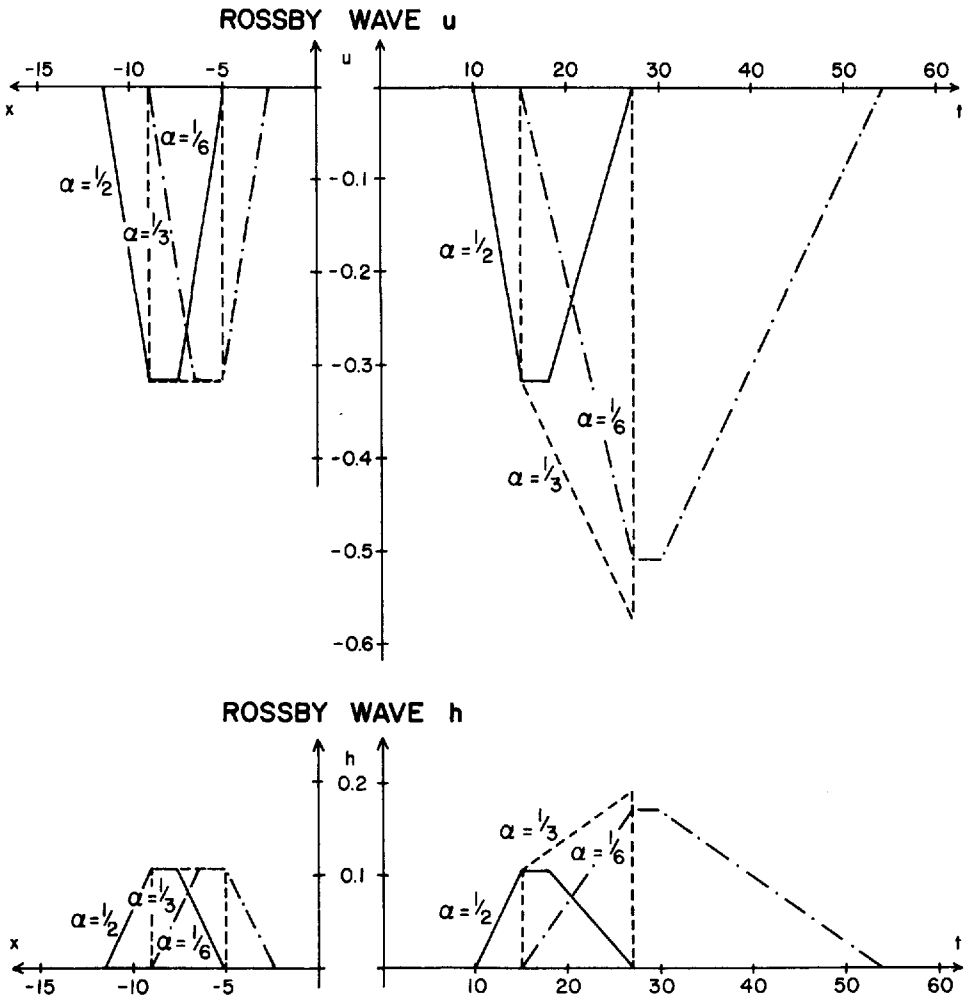

Figure 15. Rossby wave (n = 1) response in zonal velocity component, u, and upper layer thickness, h, evaluated on the equator for an easterly wind stress with constant amplitude and fetch moving westward at a rate α. Curves are given for u and h as functions of x at t = 15 for α = ⅙, ⅓ and ½.

These are shown in Figures 14–16. A Kelvin wave response only appears in and behind the forced region, while a Rossby wave response appears in the forced region and either behind it or in front of it, depending upon whether α is greater than or less than the Rossby wave group speed. When α equals the Rossby wave group speed the response is limited to the forced region and secular growth occurs since energy collects therein. Summing the two responses provides for westward progressing, abrupt, and reversing, momentum and thermal events at the leading edge of the forced region.

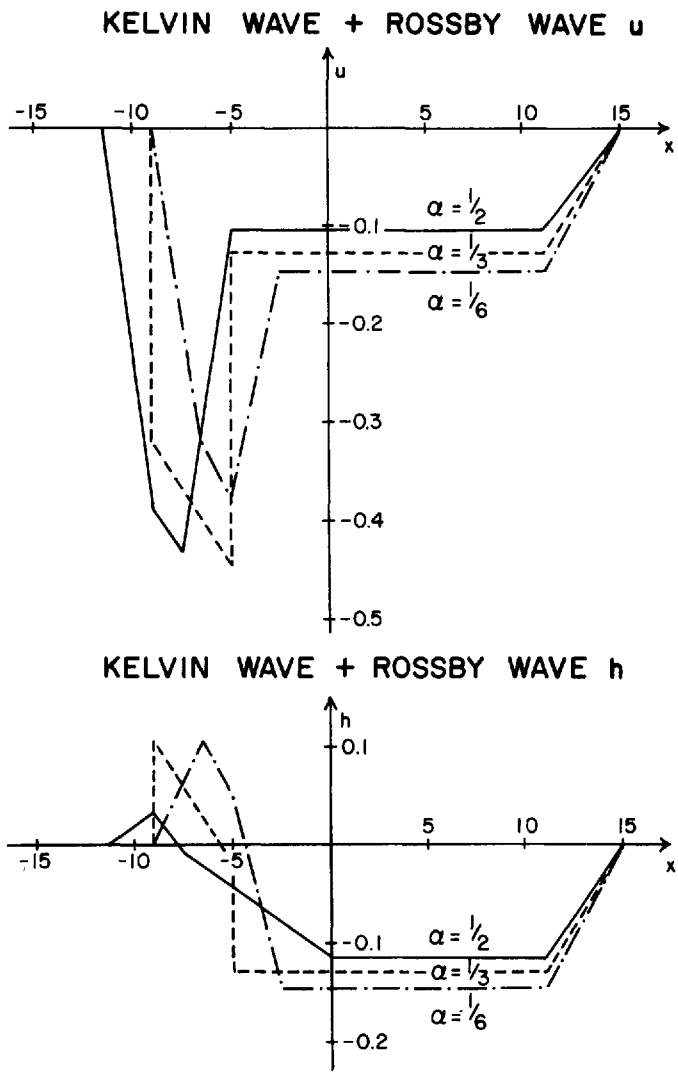

Figure 16. Sum of the Kelvin and Rossby ($n = 1$) wave responses in zonal velocity component, u, and upper layer thickness, h, evaluated on the equator for an easterly wind stress with constant amplitude and fetch moving westward at a rate α. Curves are given for u and h as functions of x at $t = 15$ for $\alpha = 1/6$, $1/3$ and $1/2$.

Perspective plots for the three cases considered are shown in Figure 17. The thermocline height is given as a function of x and t for $\alpha = 1/6$. Regions corresponding to the forcing, the Kelvin wave, and the Rossby wave are designated. The lines denoted by R and K subscripted with L and T are Rossby and Kelvin wave phase lines emanating from the leading and trailing edges of the forced region respectively.

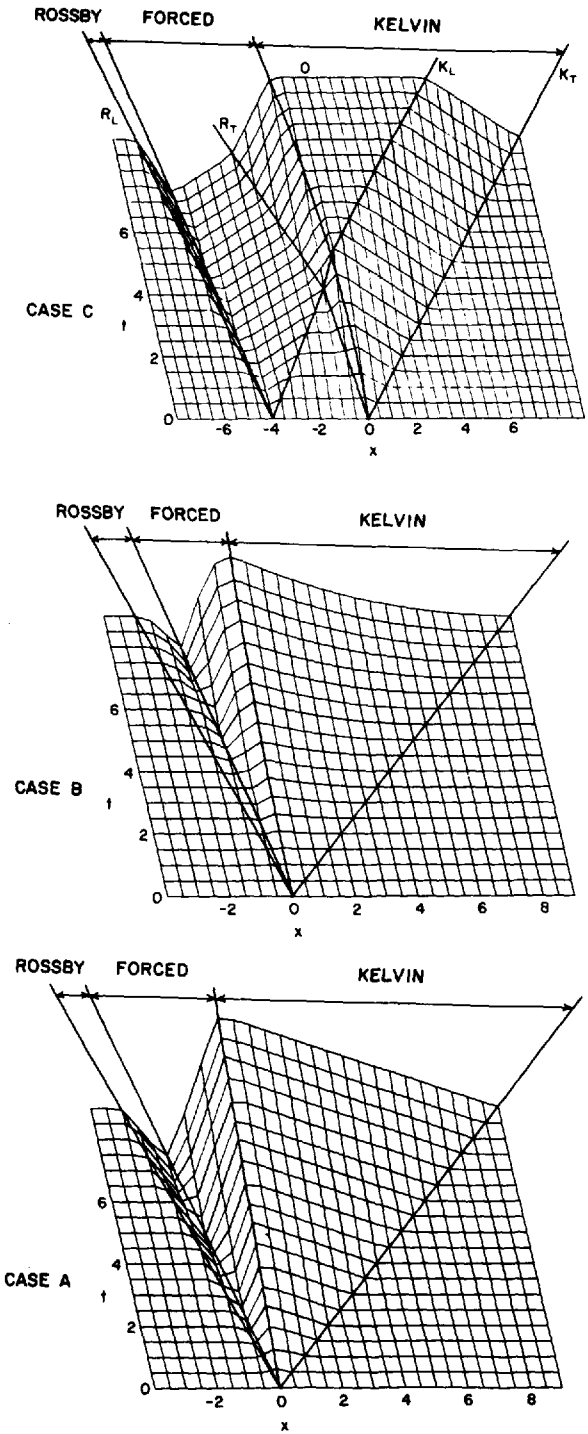

Figure 17. Sum of the Kelvin and Rossby ($n = 1$) responses in thermocline height to the three forcing functions: (A) constant amplitude with linearly expanding fetch, (B) linearly expanding amplitude and fetch, and (C) constant amplitude and fetch moving westward; are evaluated at the equator as functions x and t for $\alpha = 1/6$. Dimensions of the vertical axes are arbitrary.

4. Discussion

Figure 1 shows that the monthly mean winds over the western portion of the equatorial Atlantic are always easterly with increasing magnitude toward the west. Both the amplitude of the seasonal intensification and the duration over which this occurs also increase westward. Thus, the winds do not turn on instantaneously as modelled in Section 3. To assess the effect of this complication we've used the quadratic zonal stress distribution, $\tau(x, y, t) = \gamma \exp(-b^2y^2)x(x + \alpha t)\ H(x + \alpha t)\ H(-x)$, which builds up smoothly from the leading edge to a maximum at the center and then drops back to zero at the origin while expanding westward in both amplitude and fetch. Results similar to those of Section 3 were obtained with the exception that the forced Rossby wave response was largest at a point midway between the leading edge and the stress maximum at the center. Case b of Section 3 would therefore seem appropriate for calculating the qualitative effect of the zonal wind stress shown in Figure 1 with the instantaneous change in stress corresponding to the midpoint of the more gradual observed intensification.

Along with the forcing function simplifications we've also neglected the role of rigid meridional boundaries. One immediate consequence is the arrest of the seasonal thermocline uplift observed in Figure 4. Secular growth of the Kelvin wave response at the origin of the forced region will proceed until the fetch expands to a western boundary and the furthest portion of the Kelvin wave response propagates back to the origin. Calculating a value of the fetch expansion rate using the mid-points of the 0W–10W and 30W–40W curves of Figure 1 gives $\alpha = 1/2$, suggesting secular growth for around two months by this mechanism alone.

Variations observed at the EUC level described in Section 2 would also seem to rely on meridional boundaries. Assuming the midpoint of the 30W–40W curve in Figure 1 as being indicative of the onset time for zonal wind stress build-up upon the western boundary, we would expect to see the EUC adjust to an increased pressure gradient driving force at 26W early in July, and for this adjustment to then proceed eastward as a free Kelvin wave as observed between 26W and 24W. Similar arguments were used by Cane (1980) in his discussion of near-surface currents in the Indian Ocean using a numerical model with two active layers capable of producing an undercurrent. If the base of mixed layer becomes elevated due to waves forced by the expanding fetch, then a subsequent increase in the EUC due to a pressure gradient buildup from the western boundary might result in a critical bulk Richardson number beyond which mass and momentum mix upward and the EUC surfaces. If these suppositions are correct, then responses both internal to the equatorial ocean basin-and those propagating in from meridional boundaries are of equal footing in their effects upon SST in the central Atlantic. The internal responses can raise the thermocline while the boundary responses can both arrest this rise and increase the EUC momentum to a point at which it mixes upward and surfaces.

5. Summary

We've concerned ourselves with two aspects of the seasonal variability in the equatorial Atlantic Ocean: 1) a region of maximum seasonal upwelling along the equator between 6W–12W and 2) westward progressing thermal and momentum events which we surmised as being associated with the spatial and temporal nonuniformity of the seasonal increase in zonal wind stress. Diagnostic calculations were performed investigating the response of an unbounded, reduced gravity, equatorial β-plane ocean to expanding and moving zonal wind stress systems using techniques outlined by Cane and Sarachik (1976). Features qualitatively similar to those observed were produced. Differences arising from the neglect of meridional boundaries were discussed and it would seem plausible that in the Atlantic (where the zonal wind stress component expands in fetch and magnitude westward from the prime meridian) the ocean's responses internal to the basin and independent of meridional boundaries may be equally important as responses directly associated with the boundaries. Specifically, the region of maximum thermocline upwelling around 6W–12W may be a feature associated with the origin of the zonal wind stress, and the westward progressing thermal and momentum events may be features associated with the expanding fetch. By raising the thermocline, these effects ripen conditions for subsequent surfacing of the EUC after its zonal pressure gradient driving force expands eastward from the western boundary. The combined mechanisms can then result in the minimum SST observed between 6W–12W around July.

Since the variability of the trade wind forcing over the eastern equatorial Pacific Ocean possesses similarities with that over the Atlantic Ocean, the ideas embodied herein may have applicability to the seasonal formation of cold pools observed there.

Acknowledgments. R. Houghton and L. Miller kindly provided figures from unpublished work. The moored current meter data collection and subsequent analyses were supported by a National Science Foundation grant number OCE-7923335 as was Mr. Tang's graduate student assistantship at the North Carolina State University. Ms. T. Clay assisted with figure preparation.

REFERENCES

Adamec, D. and J. J. O'Brien. 1978. The seasonal upwelling in the Gulf of Guinea due to remote forcing. J. Phys. Oceanogr., *8,* 1050–1060.

Busalacchi, A. T. and J. J. O'Brien. 1980. The seasonal variability in a model of the tropical Pacific. J. Phys. Oceanogr., *10,* 1929–1951.

—— 1981. Interannual variability of the equatorial Pacific in the 1960's. J. Geophys. Res., *86,* 10901–10907.

Cane, M. A. 1980. On the dynamics of equatorial currents, with application to the Indian Ocean. Deep-Sea Res., *27,* 525–544.

Cane, M. and E. S. Sarachik. 1976. Forced baroclinic ocean motions. I. The linear equatorial unbounded case. J. Mar. Res., *34,* 629–665.

—— 1981. The periodic response of a linear baroclinic equatorial ocean. J. Mar. Res., *39,* 651–693.

Gill, A. E. and E. H. Schumann. 1974. The generation of long self waves by the wind. J. Phys. Oceanogr., *4,* 83–90.

Hastenrath, S. and P. J. Lamb. 1977. Climatic Atlas of the Tropical Atlantic and Eastern Pacific Ocean. The University of Wisconsin Press. 25 pages, 97 charts.

Hellerman, S. 1979. Charts of the variability of the wind stress over the tropical Atlantic. Deep-Sea Res., *26,* (Suppl. II), 63–75.

Horel, J. D. 1982. On the annual cycle of the tropical Pacific atmosphere and ocean. Mon. Weather Rev., *110,* 1863–1878.

Houghton, R. W. 1983. The subsurface thermal structure in the Gulf of Guinea. J. Phys. Oceanogr., (submitted).

Hurlburt, H. E., J. C. Kindle and J. J. O'Brien. 1976. A numerical simulation of the onset of El Nino. J. Phys. Oceanogr., *6,* 621–631.

Ichiye, T. 1959. On long waves in a stratified equatorial ocean caused by a traveling disturbance. Deep-Sea Res., *6,* 16–37.

Katz, E. J. 1981. Dynamic topography of the sea surface in the equatorial Atlantic. J. Mar. Res., *39,* 53–63.

Katz, E. J. and Collaborators. 1977. Zonal pressure gradient along the equatorial Atlantic. J. Mar. Res., *35,* 293–307.

Katz, E. J. and S. Garzoli. 1982. Response of the western equatorial Atlantic Ocean to an annual wind cycle. J. Mar. Res., *40,* (Suppl.), 307–327.

Matsuno, T. 1966. Quasi-geostrophic motions in the equatorial area. J. Met. Soc. Japan, *44,* 25–43.

McCreary, J. P. 1976. Eastern tropical ocean response to changing wind systems: with applications to El Nino. J. Phys. Oceanogr., *6,* 632–645.

Merle, J. 1978. Atlas Hydrologique Saisonnier de l'Ocean Atlantique intertropical. Trav. Doc. ORSTOM, *82,* 184, 153 pp.

—— 1980. Seasonal heat budget in the equatorial Atlantic. J. Phys. Oceanogr., *10,* 464–469.

Meyers, G. 1982. Interannual variation in sea level near Truk Island—a bimodal seasonal cycle. J. Phys. Oceanogr. *12,* 1161–1168.

Moore, D., P. Hisard, J. McCreary, J. Merle, J. O'Brien, J. Picaut, Jean-Marc Verstraete and C. Wunsch. 1978. Equatorial adjustment in the eastern Atlantic. Geophys. Res. Lett., *8,* 637–640.

Philander, S. G. H. 1981. The response of equatorial oceans to a relaxation of the trade winds. J. Phys. Oceanogr., *11,* 176–189.

Philander, S. G. H. and R. C. Pacanowski. 1980. The generation and decay of equatorial currents. J. Geophys. Res., *85,* 1123–1136.

—— 1981. Response of equatorial oceans to periodic forcing. J. Geophys. Res., *86,* 1903–1916.

Picaut, J. 1983. Propagation of the seasonal upwelling in the eastern equatorial Atlantic. J. Phys. Oceanogr., *13,* 18–37.

Received: *16 November, 1982;* revised: *11 April, 1983.*